



Master's Thesis

UWB leaky lens antenna design and simulation for waveguide measurements

By

Liu Jin

Department of Electrical and Information Technology

Faculty of Engineering, LTH, Lund University

SE-221 00 Lund, Sweden

Supervisors: Mats Gustafsson and Iman Vakili

Examinator: Daniel Sjöberg

Abstract

An ultra-wide band leaky lens antenna is designed and simulated in a parallel-plate waveguide which can work properly in the frequency range 5-30GHz in CST. The design theory is based on leaky wave propagation and the focusing property of lenses. Moreover, an air gap between the slot and the lens is introduced in order to increase the directivity of the antenna and matching layers are used to minimize the reflection coefficient and maximize the transmission coefficient. Compared with the other UWB antennas such as TEM horn antennas, the leaky lens antenna is able to achieve non-dispersive radiation over decades of bandwidth due to the constant phase center and linear phase variation. It is illustrated that the antenna is able to radiate over the interested bandwidth with less than -10dB reflection coefficient.

Acknowledgments

First of all, I want to thank my supervisors Prof. Mats Gustafsson and Iman Vakili for offering me the opportunity to become their student. I am honored very much. When I face problems, they are always patient to help me. I am grateful for their help from the bottom of my heart. Moreover, I learned a lot of good personalities and attitudes from them, which will help me in the further life.

I want to thank my examiner Prof. Daniel Sjöberg for his valuable comments and suggestions about my thesis. I appreciate his time very much.

I want to thank my university and faculty for providing me the best facility and environment.

Finally, I want to thank my mother, father, uncle for their great love. Without them, I cannot gain so much happiness.

Table of Contents

Abstract	I
Acknowledgments	III
Table of Contents	III
1 Introduction	1
2 Background Knowledge	3
2.1 UWB Technology.....	3
2.2 Directivity, Gain and Efficiency.....	4
2.3 Attenuation	5
2.4 Electromagnetic Wave Basics.....	6
3 Antenna Design and Simulation Result	9
3.1 Feeding Structure	9
3.1.1 Leaky wave antenna.....	9
3.1.2 Prototype of the leaky lens antenna.....	10
3.1.3 Concept of shadow boundary and leaky wave angle	10
3.1.4 Calculation of leaky wave angle and the role of the separation layer.....	11
3.1.5 The parameters of the feeding structure	14
3.1.6 Simulation result of the feeding structure	19
3.2 Lens Design and Simulation	23
3.2.1 Design theory of elliptical lens	23
3.2.2 Simulation result of elliptical lens model	25
3.2.3 Design theory of extended semi-circular lens.....	27
3.2.4 Simulation result of extended semi-circular lens model.....	28
3.2.5 Discussion and comparison of the two types of lens	29
3.3 Matching Layer.....	31
3.3.1 Theory of matching layer	31
3.3.2 Simulation result of the leaky lens antenna with matching layers.....	41
4 Conclusion and Future Work	44

List of Figures

Fig. 1. An example of waveguide measurement for TEM horn antennas.....2

Fig. 2. An example of leaky wave antenna.....9

Fig. 3. Illustration of a leaky lens antenna.....10

Fig. 4. Shadow boundary and leaky wave angle, θ_010

Fig. 5. A simple model with Separation Layer.....11

Fig. 6. Simple model without separation layer, back view.....12

Fig. 7. Simple model with separation layer, back view.....13

Fig. 8. Model of the leaky wave feeding structure.....14

Fig. 9. Side view of microstrip line.....15

Fig. 10. Continuous taper and multi-section taper.....17

Fig. 11. Tapered microstrip line.....18

Fig. 12. Side view of the feeding structure.....18

Fig. 13. Port signal of the feeding structure.....19

Fig. 14. S11 of feeding structure.....19

Fig. 15. VSWR of feeding structure.....20

Fig. 16. Smith chart of feeding structure.....20

Fig. 17. Impedance of feeding structure.....20

Fig. 18. Illustration of the leaky wave propagation of the feeding structure at 15GH.....21

Fig. 19. Power flow distributions at different distances away from the bottom of the lens at 15GHz.....21

Fig. 20. Elliptical lens design.....23

Fig. 21. Elliptical lens model.....25

Fig. 22. S11 of elliptical lens model.....25

Fig. 23. Impedance of elliptical lens model.....26

Fig. 24. Illustration of the E-field view of leaky wave propagation in the Elliptical Lens Model at 30 GHz.....26

Fig. 25. Extended semi-circular lens design.....27

Fig. 26. Extended semi-circular lens design Model.....27

Fig. 27. S11 of extended semi-circular lens model.....28

Fig. 28. Impedance of extended semi-circular lens.....28

Fig. 29. Illustration of the E-field view of leaky wave propagation in the extended semi-circular lens model at 30 GHz.....29

Fig. 30. Contrast of approximations among different permittivity.....	31
Fig. 31. Simple model without matching layer.....	32
Fig. 32. Simple model with one matching layer.....	32
Fig. 33. Simple model with two matching layers.....	36
Fig. 34. Reflection coefficients comparison of different matching layers...	37
Fig. 35. Reflection coefficients of matched and de-matched single matching layer.....	39
Fig. 36. Reflection coefficients with different matching layers.....	39
Fig. 37. Transmission coefficients with different matching layers.....	40
Fig. 38. Leaky lens antenna with matching layer.....	41
Fig. 39. S11 of leaky lens antenna with matching layers.....	42
Fig. 40. Impedance of leaky lens antenna with matching layers.....	43
Fig. 41. Power flow distribution comparison at 25GHz.....	43

List of Tables

Table 1. Parameters of the feeding structure.....	17
Table 2. Parameters of the matching layers.....	39

Chapter 1

1. Introduction

Ultra-wideband (UWB) antennas are commonly used in modern communications, especially for short-range high-speed indoor applications [1]. The innovation and development is witnessed over last decades. Recently, the United States Federal Communications opened the spectrum from 3-10GHz, permitting UWB technology as a new unlicensed radio transmission. Antennas act like filters and are critical elements in the signal flow for UWB systems [2]. A major problem with many pulse-based or time domain UWB antennas is dispersion. An efficient UWB antenna should be able to support non dispersive link over decades of bandwidth.

The goal of the paper is to model and simulate a novel UWB antenna in a parallel-plate waveguide which can work properly in the frequency range 5-30GHz. Fig.1 shows an example of the parallel-plate waveguide measurement of TEM horn antennas. Two TEM horn antennas are linked to the SMA connectors and used to feed the waveguide. The separation of the two parallel plates is designed to prevent the first higher mode transmission [3]. The waveguide design in our case is based on this setup.

The basic concept is to combine leaky wave propagation with a lens into a leaky lens antenna which has been proposed by Neto [4]. The design consists of three parts: feeding structure, lens and matching layers. All the designs and simulations are done in CST microwave studio. The thesis is organized in four chapters as below,

Chapter1: An overview of the thesis;

Chapter2: Introducing fundamental knowledge about UWB, antenna parameters, attenuation and electromagnetic theory;

Chapter3: Illustrating the antenna design, model and simulation;

Chapter4: Conclusion and future work.

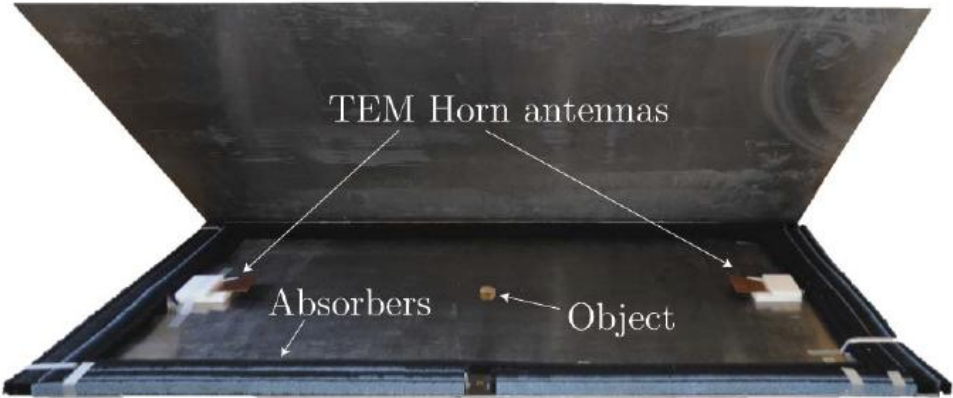


Fig.1 An example of waveguide measurement for TEM horn antennas.

Chapter 2

2. Background Knowledge

2.1 UWB Technology

Ultra Wide Band (UWB) technology plays an important role in modern communications. In UWB Technology digital data are transmitted over a wide spectrum of frequency bands with very low power [5]. Normally there are two definitions about the bandwidth of UWB. The first one refers to the absolute bandwidth larger than 500MHz; the second one refers to the relative bandwidth more than 20% [6]. UWB technology is targeted for short-range, high speed, indoor communications [1]. With the help of frequency-hopping and direct-sequence technology, the signal could be spread over a larger bandwidth with low amplitude, even lower than the noise [6].

There are many benefits of UWB technology. Firstly, the ultra wide bandwidth can achieve huge capacity up to several Gbps with distances of 1 to 10 meters. Secondly, the bandwidth can be shared to other users. Thirdly, UWB signal makes the unintended detection very difficult due to its noise-like character, which provides high security [5].

Dispersion is a big problem for pulse-based UWB system. In UWB system, propagation effects are different depending on the frequency [7]. For example, the reflection coefficient of the same objective is different at 1MHz compared with 1 GHz. Path loss is a function of frequency if the antenna gain is constant or frequency independent. The higher frequency components of the transmitted signal are attenuated more quickly compared to the lower frequency components. This leads to a distortion of individual multipath components since any frequency dependent transfer function leads to delay dispersion [6]. On the other hand, all frequency components of a signal are delayed when passed through a device. This delay will be a

constant delay for all frequencies. However, the signal delay will be different for the different frequencies unless the device has the property of linear phase. The different delay for different frequency will induce the distortion of the output signal. As the result, the signal shape is changed in addition to the constant delay or scale change. If the phase center is constant and variation of the phase is linear as a function of frequency, this device can be viewed as non dispersive [4].

2.2 Directivity, Gain and Efficiency

As it is known to us from the law of conservation of energy, the total energy remains constant in a system. The effect of the antenna is to redistribute the energy and concentrate it in one direction.

The directivity and gain are two of the most important parameters of an antenna. Directivity of an antenna is defined as “the ratio of maximum radiation power to the radiation power averaged over all directions” [8]. In mathematical form, it can be written as

$$D = \frac{P_{\max}}{P_{\text{average}}} \quad (2.1)$$

Directivity is a value ≥ 1 . The average radiation power is equal to the total radiated power divided by 4π .

The gain of antenna is an actual or realized quantity which is less than directivity due to the ohmic losses in the antenna. Part of the energy is not radiated but converted to thermal energy [8]. The relation of the directivity and gain can be written as[9]

$$G=k \cdot D \quad (2.2)$$

where k refers to the efficiency factor without concerning reflection loss ($0 \leq k \leq 1$). In another word, directivity is the idealized value and gain is the practical value.

Except for the thermal energy loss, another part of loss is caused by mismatched impedance. This causes reflection at the interface between the antenna and transmission line [9]. Thus, the total antenna efficiency can be written as,

$$e_0 = e_r e_c e_d \quad (2.3)$$

where e_0 is the total efficiency. e_r is the reflection efficiency which refers to reflection loss. e_c is conduction efficiency and e_d is dielectric efficiency. $k = e_c e_d$ is antenna radiation efficiency, which refers to the thermal loss [9]. The antenna efficiency measures “how efficiently” an antenna converts the input power into radiation.

For the receiving antennas, one important property is its “effective area”, which indicates the area from which the antenna can absorb the power from an incoming electromagnetic wave. The relation between effective area A_{rx} of an antenna and the receiving antenna gain can be written as,

$$G_{rx} = \frac{A_{rx}}{A_{iso}} = \frac{4\pi}{\lambda^2} A_{rx} \quad (2.4)$$

where $A_{iso} = \frac{\lambda^2}{4\pi}$ refers to the effective area of an isotropic antenna [8].

2.3 Attenuation

According to the different distances from the transmit antenna, the attenuation factor varies as a function of distance. There is a threshold distance d_{break} for each communication link. For distances $d < d_{break}$, the received power decreases as $1/d^2$, which is known as Friis’ Law [6]:

$$P_{rx} = P_{tx} G_{tx} G_{rx} \left(\frac{\lambda}{4\pi d}\right)^2 \quad (2.5)$$

The factor $(\lambda/4\pi d)^2$ is the free space loss factor. Friis’ Law is restricted to the far field of the antenna, which means the distance is greater than one Rayleigh distance [6]. The Rayleigh distance is defined as

$$d_{Rayleigh} = \frac{2L_a^2}{\lambda} \quad (2.6)$$

where L_a refers to the largest dimension of antenna. By Friis' Law, it is easy to know that high frequency components decay much faster than the low frequency components. This kind of loss is also called free space loss. However, for distances $d > d_{\text{break}}$, the received power decreases as $1/d^4$ [6], which can be written as:

$$P_{\text{rx}} = P_{\text{tx}} G_{\text{tx}} G_{\text{rx}} \left(\frac{h_{\text{tx}} h_{\text{rx}}}{d^2} \right)^2 \quad (2.7)$$

where h_{tx} and h_{rx} are the height of the transmitting and receiving antenna. The threshold d_{break} is defined as [6]:

$$d_{\text{break}} = \frac{4h_{\text{tx}} h_{\text{rx}}}{\lambda} \quad (2.8)$$

This equation implies that the threshold d_{break} is different for different frequencies. The higher frequency component has a farther d_{break} distance. This distance is called the breakpoint of the link. In real situations, there is one more breakpoint where the received power decays much faster than $1/d^4$. The reason can be explained by radio horizon effect.

2.4 Electromagnetic Wave Basics

In this subchapter, some fundamental equations and concepts of electromagnetic wave are introduced.

Wavenumber

Wavenumber k describes the number of wavelengths in a 2π distance [10], which can be written as

$$k = \frac{2\pi}{\lambda} \quad (2.9)$$

Assume there are two different medium, v represents the wave speed in the medium and n is the refractive index. They satisfy the following equation [11]:

$$\frac{n_2}{n_1} = \frac{k_2}{k_1} = \frac{v_1}{v_2} = \frac{\lambda_1}{\lambda_2} \quad (2.10)$$

Eq. (2.10) explains the relationship among different parameters, which aids the further calculations in chapter 3.

Refractive Index, Permittivity and Characteristic Impedance

The speed of light in the material can be written in form of the absolute permittivity and permeability [11].

$$v = \frac{1}{\sqrt{\mu\varepsilon}} \quad (2.11)$$

where the μ is the absolute permeability and ε is the absolute permittivity. Let μ_0 and ε_0 denote the permittivity and permeability of vacuum, thus speed of light can be written in form of the relative permittivity and permeability [11].

$$v = \frac{1}{\sqrt{\mu_r \varepsilon_r \mu_0 \varepsilon_0}} \quad (2.12)$$

According to Eq. (2.11), the speed of light in vacuum can be written as

$$v_0 = \frac{1}{\sqrt{\mu_0 \varepsilon_0}} \quad (2.13)$$

By combining Eq. (2.12) and Eq. (2.13), the refractive index can be written as

$$n = \frac{v_0}{v} = \sqrt{\mu_r \varepsilon_r} \quad (2.14)$$

For the non-magnetic material, we have $\mu_r = 1$ [11]. Thus,

$$n = \sqrt{\varepsilon_r} \quad (2.15)$$

This equation gives the relationship between the refractive index and permittivity of one medium. Similarly, the characteristic impedance of one medium can be written in form of corresponding vacuum value and refractive index [11],

$$\eta = \sqrt{\frac{\mu}{\varepsilon}} = \sqrt{\frac{\mu_r \mu_0}{\varepsilon_r \varepsilon_0}} = \eta_0 \sqrt{\frac{\mu_r}{\varepsilon_r}} = \eta_0 \sqrt{\frac{1}{\varepsilon_r}} = \frac{\eta_0}{n} \quad (2.16)$$

It is easy to use Eq. (2.16) to get that the characteristic impedance is inversely proportional to the refractive index.

$$\frac{\eta_1}{\eta_2} = \frac{n_2}{n_1} \quad (2.17)$$

TEM, TE and TM Waves

When the electromagnetic wave is propagating in a parallel-plate waveguide, there are many different modes transmitting simultaneously. The basic mode is the TEM mode, which means that there are neither electric nor magnetic field in the direction of propagation [12]. In another word, the E field and H field were both perpendicular to the direction of propagation [13]. TEM waves propagate at all frequencies. TE mode means that there is no E-field in the direction of propagation and TM mode means no H-field in the direction of propagation [12]. Both of them are higher-order mode propagations. As the frequencies become higher, higher-order mode will be excited [13]. As a result, for each mode there will be a corresponding cut-off frequency. All these cut-off frequencies are solutions to eigenvalue problems that satisfy the boundary conditions [14]. For the case of the parallel-plate waveguide, the cutoff frequencies for the TE modes are the same as for the TM modes, which can be expressed as [3],

$$f_c = \frac{v}{2d} n = \frac{n}{2d\sqrt{\mu\epsilon}} \quad (2.18)$$

Helmholtz Equations

Helmholtz equation is derived from Maxwell equations. The E field and H field must satisfy the Helmholtz equation when the electromagnetic wave is propagating inside the waveguide [12].

$$\begin{aligned} \nabla^2 E + k^2 E &= 0 \\ \nabla^2 H + k^2 H &= 0 \end{aligned} \quad (2.18)$$

where k is the wavenumber. The wavenumber can be also written in the form of the angular frequency, $k = \omega\sqrt{\mu\epsilon}$. The Helmholtz equation is often used in the problems involving partial differential equations in both space and time.

3. Antenna Design and Simulation

Result

3.1 Feeding Structure

3.1.1 Leaky wave antenna

When the electromagnetic wave is propagating along a traveling wave structure, and if this structure can cause continuous radiation from inside to outside, this structure is called leaky wave antenna and such radiation is called leaky wave.

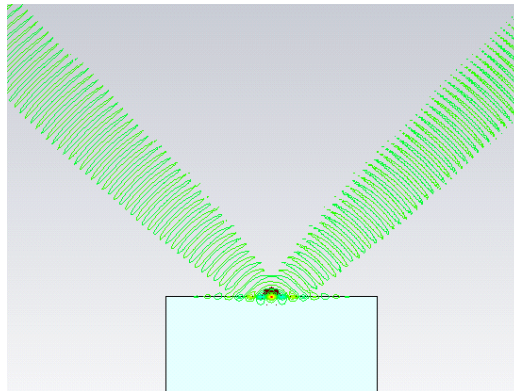


Fig. 2. An example of leaky wave antenna.

Here is one example of a leaky wave antenna. As Fig. 2 describes, an electric dipole is placed in a parallel-plate waveguide and the outer space is filled with the medium silicon. The leaky wave is generated by dipole and propagates from the waveguide slot into the dielectric silicon. The wave which is generated by the leaky wave antenna is usually a planar beam. Leaky wave antennas are a class of antennas that use a travelling wave on the guiding structure as the main radiating mechanism [15].

3.1.2 Prototype of the leaky lens antenna

In order to concentrate the ray to a specific direction, a practical way is to add a lens structure on top of the feeding structure. The leaky slot guarantees a broad bandwidth and a symmetric lens structure will lead to a symmetric radiation pattern [4]. The combination of leaky wave and lens is called leaky lens antenna. As Fig.3 shows, this is a prototype of the leaky lens antenna. The lens part is able to capture the rays and focus them in one direction. The section from B to B' is the focus area, the other part of the rays are lost in spill over since they are scattered in useless directions [5]. Our design originates from this prototype and the discussion about the contrast the two types of the lens structure is in Chapter 3.2.

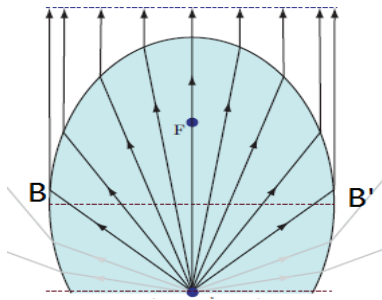


Fig. 3. Illustration of a leaky lens antenna.

3.1.3 Concept of shadow boundary and leaky wave angle

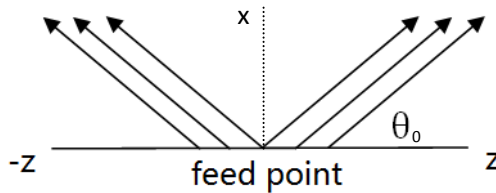


Fig. 4. Shadow boundary and leaky wave angle, θ_0 .

Fig. 4 illustrates an example of near field leaky wave radiation. It is very hard to clearly observe the leaky wave in the far field because it attenuates exponentially in both directions, $z = \pm \infty$. The leaky wave radiation is symmetric about the x-axis. There is a specific angle θ_0 for each model.

When $\theta = \theta_0$, the strength of the leaky wave is the strongest. When θ deviates from θ_0 , the strength of the leaky wave will decrease. This angle is called leaky wave angle. And the boundary of this specific θ_0 is called “shadow boundary”. The field strength increases significantly from $\theta = 0^\circ$ up to the leaky wave angle and decrease rapidly above the shadow boundary [16]. The calculation method of leaky wave angle is discussed in Chapter 3.1.4.

3.1.4 Calculation of leaky wave angle and the role of the separation layer

Due to the symmetry of the leaky wave in the lens structure, the angle separating the two leaky wave beams is $(\pi - 2 * \theta_0)$. However, a large separating angle is not acceptable because that will induce a high side lobe level.

In order to get a good performance, an effective way is to increase the leaky wave angle as much as possible. In another word, the closer the two beams, the better the result is. In this way, a main beam can be combined with low side lobe. From previous research [4], one result states that any leaky wave angle smaller than 70° will induce side lobes higher than -10dB. Based on this, the minimum requirement of the leaky wave angle for this design is 70° .

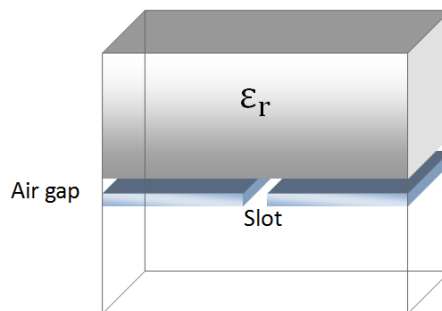


Fig. 5. A simple model with separation layer.

Fig. 5 shows a simple model of a leaky wave with separation layer structure. The sequence from up to down is as following, dielectric part, air gap, slot layer, and air. The air gap separates the dielectric part and slot layer that's why we call it separation layer. Leaky wave is generated from the slot and can be calculated by Eq. (3.1).

$$\theta_0 = \cos^{-1}(\beta/k_2) \quad (3.1)$$

The leaky wave angle with and without air gap are compared as below. Assume the wavenumber in media air is k_1 and the wavenumber in the media of the lens is k_2 . The propagation constant of the slot is the parameter β . The leaky wave angle is the parameter θ_0 and $\epsilon_1 = 1$.

For the model without the separation layer:

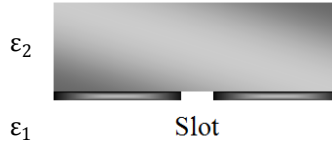


Fig. 6. Simple model without separation layer, back view.

Since the slot at the interface of the two medium, the equation of the propagation constant at the slot is [4]

$$\beta = \sqrt{(k_1^2 + k_2^2)/2} \quad (3.2)$$

Resulting from Eq. (3.1) and Eq. (3.2):

$$\theta_0 = \cos^{-1}\left(\sqrt{\frac{k_1^2 + k_2^2}{2}}/k_2\right) \quad (3.3)$$

$$\theta_0 = \cos^{-1}\left(\sqrt{\frac{k_1^2 + k_2^2}{2 * k_2^2}}\right) \quad (3.4)$$

$$\theta_0 = \cos^{-1}\left(\sqrt{\frac{k_1^2}{2 * k_2^2} + \frac{1}{2}}\right) \quad (3.5)$$

Due to $\frac{k_1^2}{2 * k_2^2} > 0$, the maximum value of θ_0 is 45° .

For the model with the separation layer:

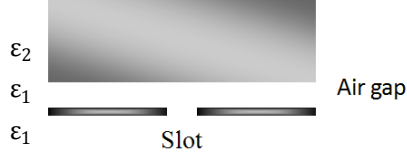


Fig. 7. Simple model with separation layer, back view.

Since the slot is fully inside the medium of air in this case, the propagation constant is $\beta \approx k_1$, thus the leaky wave angle in this case is:

$$\theta_0 = \cos^{-1}(k_1/k_2) \quad (3.6)$$

By Eq. (2.10) and Eq. (2.15), we obtain:

$$\theta_0 = \cos^{-1}\left(\frac{1}{\sqrt{\epsilon_r}}\right) \quad (3.7)$$

Comparing Eq. (3.5) and Eq. (3.7), it is obvious that in this simple leaky lens model, the separation layer plays an important role which can enhance the leaky wave angle effectively. In the model without the separation layer, the largest angle between the two beams is 90° . However, as long as a reasonable and proper ϵ_r is set, the leaky wave angle can be larger than 70° .

Firstly we choose a lens material named “porcelain”, the relative permittivity of 6. However, in this way the leaky wave angle is only around 65° . It is still a little lower than the threshold 70° . Finally “silicon” is used as lens material, the permittivity of which is 11.67. The leaky wave angle is around 73° , which can satisfy the requirement.

3.1.5 The parameters of the feeding structure

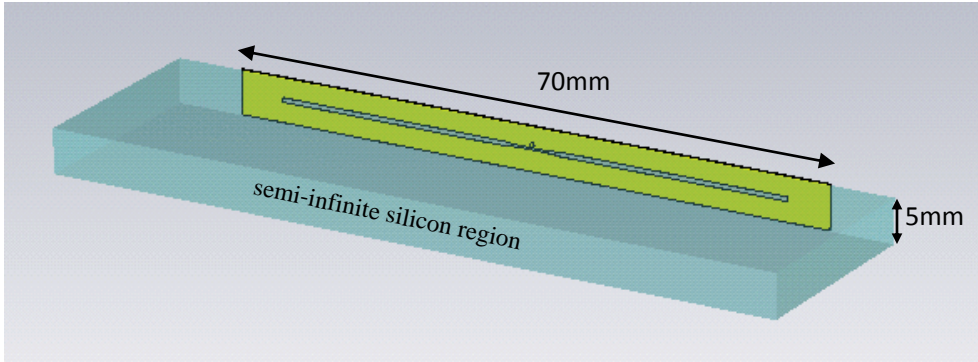


Fig. 8. Model of the leaky wave feeding structure.

The Fig. 8 shows an overview of the leaky wave feeding structure model. The feeding structure is the foundation of the antenna. The goal is to lower the reflection coefficient curve as much as possible. That is because after adding the lens part on top of the feeding structure in the next step, the level of the reflection coefficient curve will increase due to the reflection of the lens-air interface. The lens part in this model is assumed as semi-infinite space in the direction of the leaky wave propagation.

Due to the simulation in a parallel-plate waveguide, the first thing is to determine the distance d between the top and bottom plates in the parallel-plate waveguide. The distance is calculated by Eq. (3.8) and Eq. (3.9), which is derived from Eq. (2.18) [17].

$$c = \lambda_c * f_c \quad (3.8)$$

$$\lambda_c = 2 * d \quad (3.9)$$

The model is designed to work excellently in the frequency range 5-30GHz, thus the cutoff frequency should be 30GHz to prevent the first higher mode transmission. λ_c is the corresponding wavelength of this frequency. By calculation, the distance is 5mm.

The material of the substrate in the simulation is Rogers RT5880 (lossy), the relative permittivity of which is $\epsilon_r = 2.2$. Another goal of this design is to make the antenna as small as possible. Thus the thickness of the substrate

is only 0.127mm; however, this thin thickness brings a lot of difficulty in the design, for example, leading a narrow width of microstrip line, a small size of metallic via radius, a high level of reflection coefficient curve and so forth [18]. All these problems are discussed and solved in the following part of this chapter.

Another important parameter is the width of the microstrip line. This parameter is crucial to attain the impedance matching. When the impedance is matched, the reflection and mismatch loss is minimized and the transmission efficiency is maximized. In order to achieve the impedance matching, the microstrip line impedance should be $Z_L = 50\Omega$. In this section four different calculation methods for the desired characteristic impedance are introduced. Assume that w is the width of microstrip line and h is the thickness of the substrate, see Fig.9.

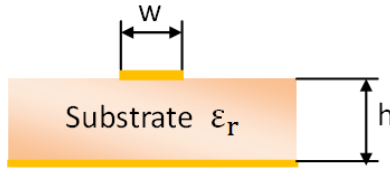


Fig. 9. Side view of microstrip line.

Wheeler

The Wheeler equation was proposed by Wheeler in 1965, which is classic and widely used in microstrip line design [19]. This equation is based on conformal mapping's approximation. The formulae are applicable to alumina-type substrates and have an estimated error less than 1 per cent.

For wide strips $\frac{w}{h} > 3.3$

$$Z_L = \frac{Z_0}{2\sqrt{\epsilon_r}} \cdot \frac{1}{\frac{w}{2h} + \frac{1}{\pi} \ln 4 + \frac{\epsilon_r + 1}{2\pi\epsilon_r} \ln\left(\frac{\pi e}{2}\left(\frac{w}{2h} + 0.94\right)\right) + \frac{\epsilon_r - 1}{2\pi\epsilon_r^2} \cdot \ln \frac{e\pi^2}{16}} \quad (3.10)$$

For narrow strips $\frac{w}{h} \leq 3.3$

$$Z_L = \frac{Z_0}{\pi\sqrt{2(\epsilon_r + 1)}} \cdot \left(\ln\left(\frac{4h}{w} + \sqrt{\left(\frac{4h}{w}\right)^2 + 2}\right) - \frac{1}{2} \cdot \frac{\epsilon_r - 1}{\epsilon_r + 1} \left(\ln \frac{\pi}{2} + \frac{1}{\epsilon_r} \ln \frac{4}{\pi} \right) \right) \quad (3.11)$$

Schneider

Schneider also proposed a microstrip line calculation formula in 1968 which is obtained by rational function approximation. The accuracy of this equation is approximately around $\pm 0.25\%$ for the range of $0 \leq w/h \leq 10$, and $\pm 1\%$ for $w/h \geq 10$ [20].

$$Z_L = \frac{Z_0}{\sqrt{\epsilon_{r\text{eff}}}} \cdot \begin{cases} \frac{1}{2\pi} \cdot \ln\left(\frac{8h}{w} + \frac{w}{4h}\right) & \text{for } \frac{w}{h} \leq 1 \\ \frac{1}{\frac{w}{h} + 2.42 - 0.44 \frac{h}{w} + \left(1 - \frac{h}{w}\right)^6} & \text{for } \frac{w}{h} > 1 \end{cases} \quad (3.12)$$

$$\epsilon_{r\text{eff}} = \frac{\epsilon_r + 1}{2} + \frac{\epsilon_r - 1}{2} \cdot \frac{1}{\sqrt{1 + 10 \frac{h}{w}}} \quad (3.13)$$

Hammerstad and Jensen

This equation was developed by E. Hammerstad and Ø. Jensen in 1980. It can also provide high accuracy. The formulae are presented for both single and coupled microstrip lines model. For the single microstrip the effects of dispersion is also included [21].

$$Z_L = \frac{Z_0}{2\pi\sqrt{\epsilon_r}} \cdot \ln\left(f_u \frac{h}{w} + \sqrt{1 + \left(\frac{2h}{w}\right)^2}\right) \quad (3.14)$$

$$f_u = 6 + (2\pi - 6) \cdot \exp\left(-\left(30.666 \cdot \frac{h}{w}\right)^{0.7528}\right) \quad (3.15)$$

John D. Kraus

$$Z_L = \frac{Z_0}{\sqrt{\epsilon_r} \left(\frac{w}{h} + 2\right)} \quad (3.16)$$

Another accurate calculation method was proposed by John D. Kraus in 1988 [22]. It simplifies the calculation process. The equations from the first two methods have their own thresholds for w/h , which is hard to decide which one is going to be used at the beginning. At last, John's equation is adopted in the design. One thing need to figure out is that all the equations of these four methods are based on an infinitely thin microstrip line thickness. To maintain the same impedance, an increased thickness will decrease the width. In our case, the thickness of the microstrip line is 0.018mm, which is negligible in the effective permittivity calculation. This gives the width of the microstrip line, $w=0.39\text{mm}$.

Eq. (3.16) implies a relatively thin substrate leading to a relatively narrow microstrip width and metallic via radius. Metallic via holes drilled and penetrated through the substrate contributes with smaller parasitic inductances to the overall performance [18]. Metallic via directly connects the slot layer and microstrip line. In order to maintain a constant impedance, a decreased thickness induce a decreased width of microstrip, as well as the radius of the metallic via, which leads to high conductor loss, low quality factor, higher reflection coefficient, high demanded fabrication, etc. [18].

Tapered Microstrip Transmission Line

Based on this, a new design element named “tapering” is introduced. Tapered microstrip transmission lines are an increasingly important part in design of matching network, filters, couplers, circulators, etc [23]. The propagation constant of a tapered microstrip line varies along its length. In general, the tapered microstrip means that the width of microstrip line is non-uniform. Depending on the different designs of the tapered shape, there are different types, for example, the exponential taper, the triangular taper, and the Klopfenstein taper, and so forth [24].

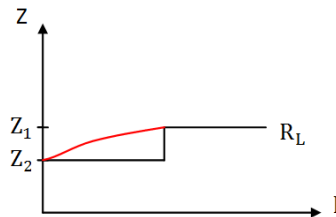


Fig. 10. Continuous taper and multi-section taper.

Fig. 10 shows the impedance shift of the tapered microstrip line. Both of the continuous impedance taper and multi-section impedance taper are feasible in tapering design. The latter one is used in this design. In order to attain the status of the impedance match at the port interface, the impedance Z_1 is fixed to 50Ω and Z_2 is the desired impedance. As a result, each section of the impedance is modified by adjusting the corresponding width of the microstrip line. Fig. 11 shows the tapered microstrip line. In this way, the problems brought by the narrow width of the microstrip line and small size of metallic via are solved.

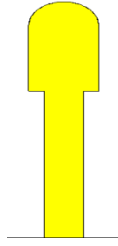


Fig. 11. Tapered microstrip line.

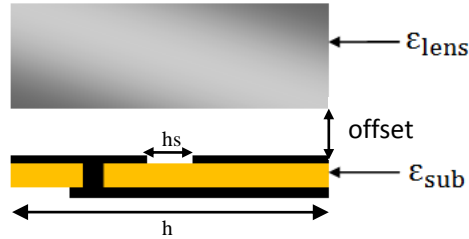


Fig. 12. Side view of the feeding structure.

h	5mm	t	0.127mm
h_s	0.5mm	t_{pec}	0.018mm
l	70mm	$w1$	0.39mm
l_s	60mm	$w2$	0.7mm
offset	0.225mm	ϵ_{sub}	2.2
R_{via}	0.25mm	ϵ_{lens}	11.67

Table 1. Parameters of the feeding structure.

Fig. 12 shows the side view of the feeding structure and table 1 gives the relevant parameter of the design. The thickness of substrate is t and the material is Rogers RT5880 (lossy). Above the substrate is the slot layer. The material of the slot layer and microstrip line is copper. The length and width of the slot are h_s and l_s . The radius of the metallic via is R_{via} . The offset means the air gap between the slot and the lens.

3.1.6 Simulation result of the feeding structure

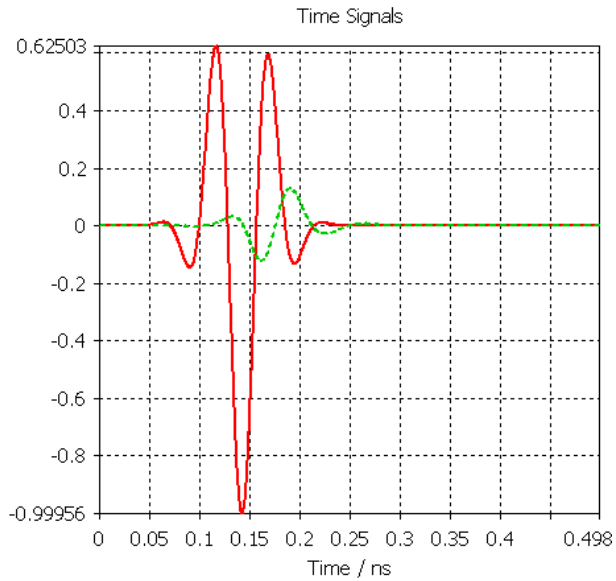


Fig. 13. Port signal of the feeding structure.

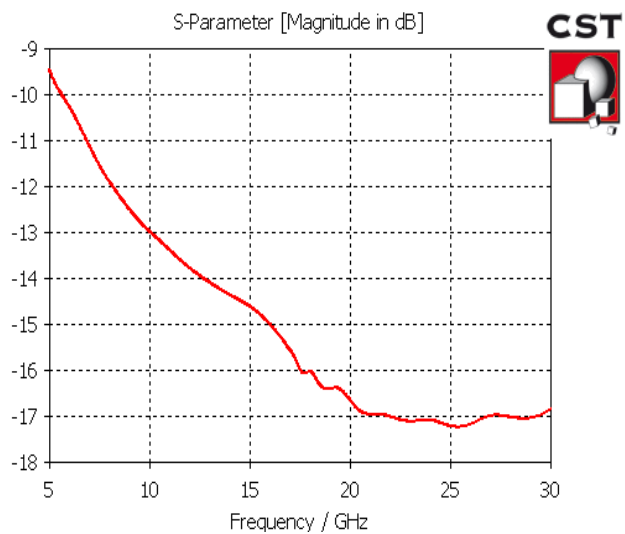


Fig. 14. S11 of the feeding structure.

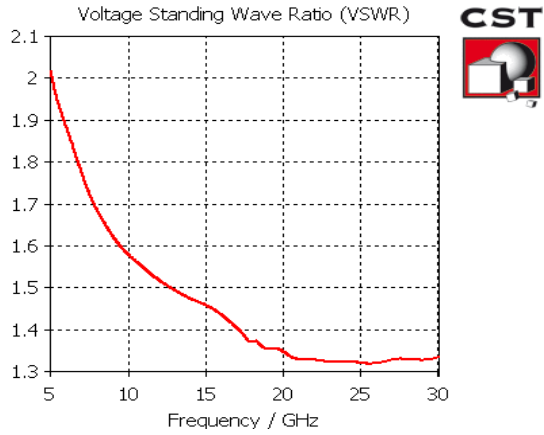


Fig. 15. VSWR of the feeding structure.

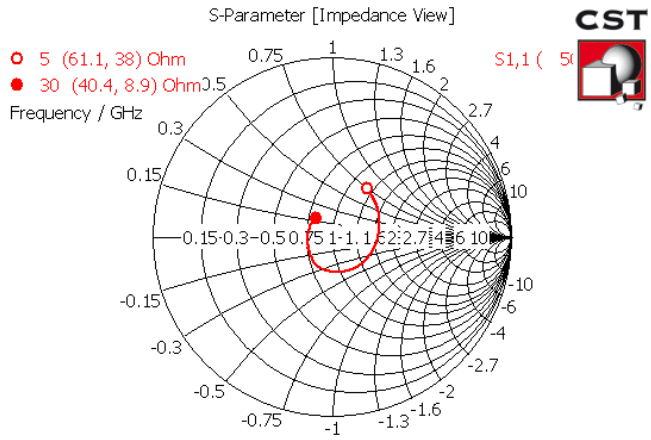


Fig. 16. Smith chart of the feeding structure.

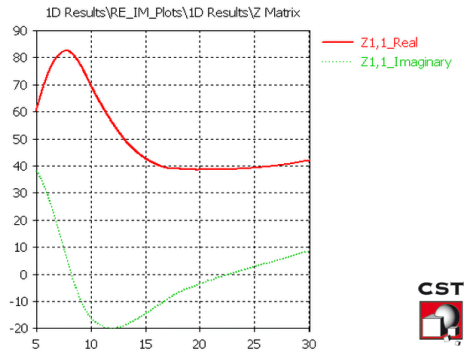


Fig. 17. Impedance of the feeding structure.

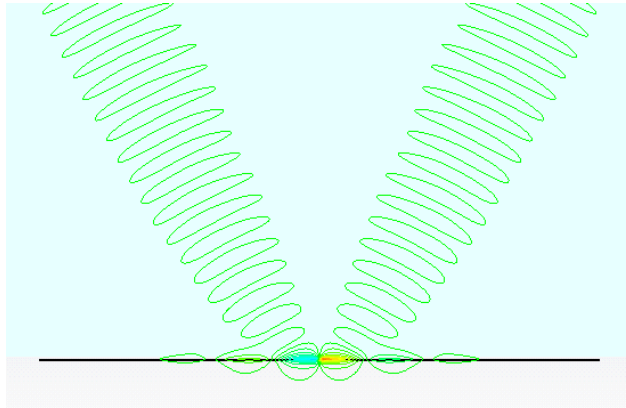


Fig. 18. Illustration of the leaky wave propagation of the feeding structure at 15GHz.

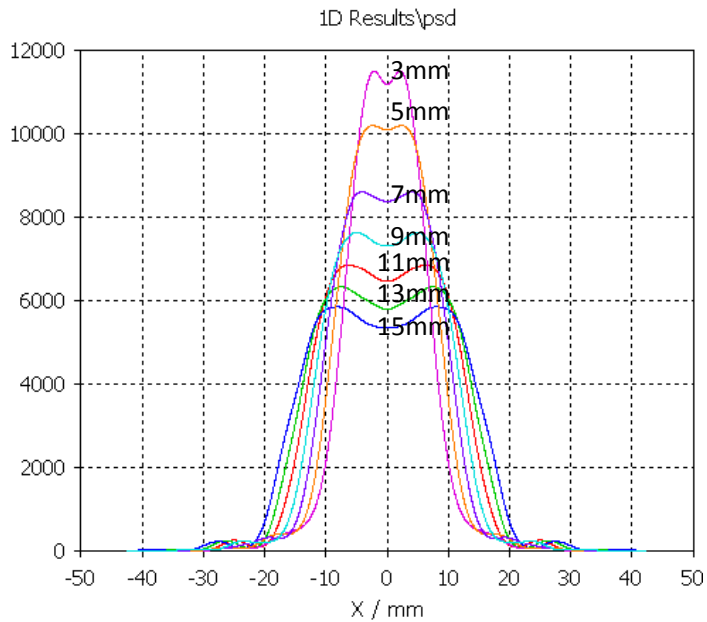


Fig. 19 Power flow distributions at different distances away from the bottom of the lens at 15GHz.

The port signal is shown in Fig. 13. The solid curve is an incident Gaussian excitation signal and the dash curve represents the reflected signal. The amplitude is normalized thus the maximal amplitude is 1. It is clear to see that the peak value of the reflected signal is constrained within 0.18.

S-parameter is the abbreviation of the scattering parameter, which shows the reflection coefficient over the considered bandwidth. It is an important parameter in measuring the antenna's performance. The amplitude is in dB value. For example, S11=0dB means all the energy is reflected without any transmission. In Fig. 14, it is clear that in the frequency band 5-30 GHz, almost all the S11 is below -10dB except for a small part around 5GHz. Compared to the lower frequency band, the performance of the higher frequency band is much better. Especially in the range of 15-30GHz, the S-parameter is even below -15dB. S-parameter is the Fourier transform of the port signal. Voltage Standing Wave Ratio (VSWR) is similar to S-parameter, which is calculated by [13]

$$VSWR = \frac{1+|\Gamma|}{1-|\Gamma|} \quad (3.17)$$

where the Γ is the reflection coefficient. The ideal case is VSWR=1, which means no reflection occurs and the impedance is matched perfectly. Thus minimal value of VSWR is 1. We cannot see the linear relation between VSWR and reflection coefficient by Eq. (3.17). However, in Fig. 15, it is interesting to see that the VSWR has the same trend as the S-parameter. They increase or decrease simultaneously.

The Smith Chart is shown in Fig. 16, which is the impedance view of S-parameter. Characteristic impedance is a complex number. The real part is resistance and the imaginary part is reactance. The Smith Chart shows the resistance and reactance in the corresponding frequency. The central point is matched impedance point, which is 50Ω in our case. The upper part represents inductive reactance and the lower part represents capacitive reactance [14]. It is clear to see the whole curve is close to the central point, which means impedance matching is roughly attained during the whole frequency band. The impedance-parameter is similar as the Smith chart but in a more directive way to see impedance at each frequency. The real part (solid curve) and the imaginary part (dotted curve) of the impedance are shown in Fig. 17. The real part is closer to 50Ω and the imaginary part is closer to 0Ω at high frequency band compared to the ones at low frequency band, that's why we got much lower reflection coefficients in the high frequency band.

As it is known to us, the elliptical lens is able to make the parallel ray converge at the focal point, or convert the ray emitted from focal point into parallel ray. This is demonstrated in the optical theory. However, visible light is one kind of electromagnetic radiation which is visible to the human. Based on this, feeding structure is designed to set in the position of the focal point of the lens, so that the leaky wave beam can be converted to the parallel beam.

According to the definition of the ellipse:

$$\left(\frac{x}{a}\right)^2 + \left(\frac{y}{b}\right)^2 = 1 \quad (3.19)$$

where a is the semi-major axis and b is the semi-minor axis. c is the focal length as seen in Fig. 20. The connection line P_1P_2 in Fig. 20 indicates the shortest focal axis, the length of which is set to $P_1P_2=70\text{mm}$.

The relation between the eccentricity of the ellipse and permittivity is

$$e = \frac{1}{\sqrt{\epsilon_{\text{lens}}}} \quad (3.20)$$

Assume $r = \frac{P_1P_2}{2}$ and $x = P_2F$, thus

$$x + r = 2b \quad (3.21)$$

$$2r = \frac{2a^2}{b} \quad (3.22)$$

$$\frac{c}{b} = e \quad (3.23)$$

$$c = \sqrt{b^2 - a^2} \quad (3.24)$$

By combing the equations from (3.20) to (3.24) [25], the dimensions of ellipse are determined as, $a=36.6\text{mm}$, $b=38.2\text{mm}$ and $c=11.2\text{mm}$. Before the simulation, the separation layer must be inserted. Thus one bottom part of the lens is replaced by a 0.225mm thick air gap. The elliptical lens model is shown in Fig.21.

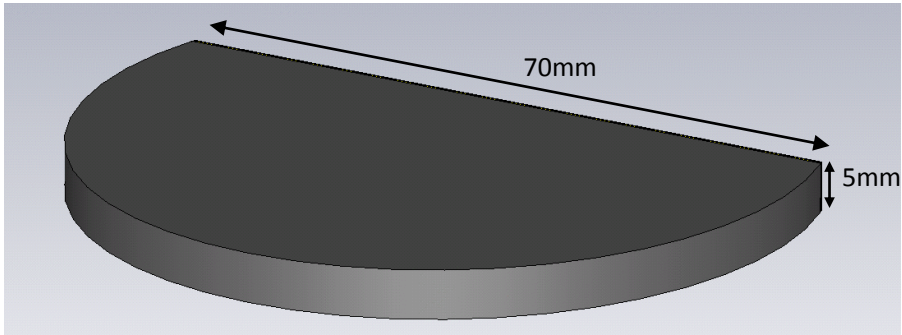


Fig. 21. Elliptical lens model.

3.2.2 Simulation result of elliptical lens model

Fig. 22 shows the S-parameter of the elliptical lens model, covering the band from 5-30GHz. It is observed that the S11 is below -10dB from 20 GHz on. However, in the range of 5-15GHz, the performance is much worse. The reflections inside the lens are very complicated, which produce rapid oscillations in S11 as a function of frequency. The impedance is shown in Fig.23. The real part is closer to 50Ω and the imaginary part is closer to 0Ω at high frequency band compared to the ones at low frequency band. The oscillations of the impedance are also caused by the reflections inside the lens. Fig. 24 shows the E-field distribution in H-plane at 30 GHz. A main beam is formed on top of the lens. In summary, the elliptical lens is designed successfully according to the calculation.

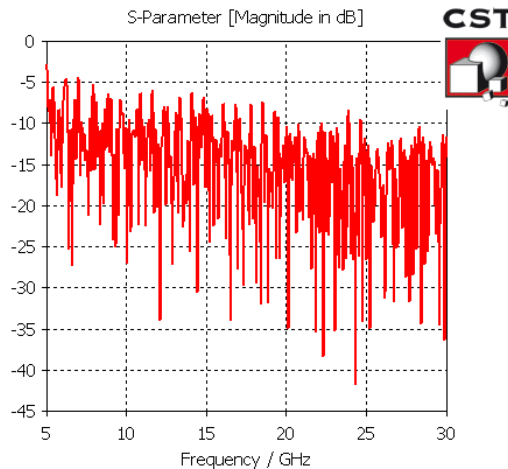


Fig. 22. S11 of elliptical lens model.

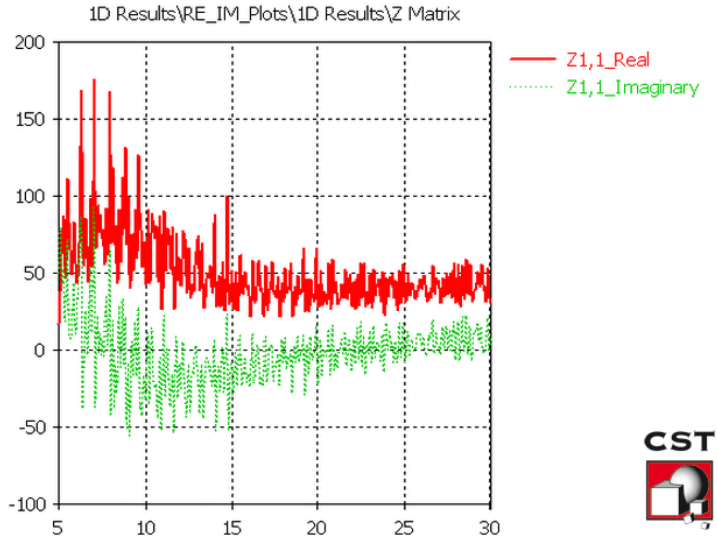


Fig. 23. Impedance of elliptical lens model.

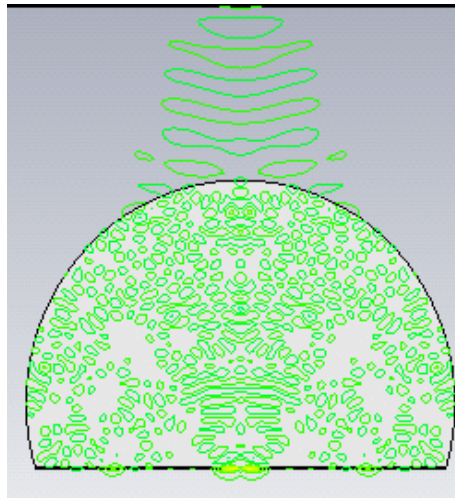


Fig. 24. Illustration of the E-field view of leaky wave propagation in the elliptical lens model at 30GHz.

3.2.3 Design theory of extended semi-circular lens

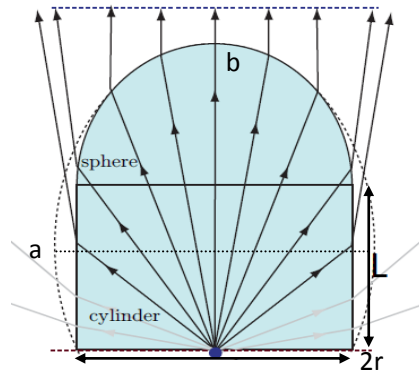


Fig.25 Extended semi-circular lens design.

In this subchapter a new type of lens will be introduced. As it is shown in Fig. 21, without changing the focus area, the elliptical lens could be replaced by a semi-circular lens with a proper extension length. In another word, the synthesis lens has the equivalent function as the elliptical lens in the focus area, so that the extension length L should be adequate to superimpose the two lenses [25], which yields:

$$L + r = b + c \quad (3.25)$$

where a is the semi-major axis and b is the semi-minor axis, and c is the focal length. By combing the equations from (3.20)-(3.25) [25], all the lens parameters are determined as, $a=36.6\text{mm}$, $b=38.2\text{mm}$, $c=11.2\text{mm}$ and $L=14.5\text{mm}$. The extended semi-circular lens model is presented in Fig. 26.

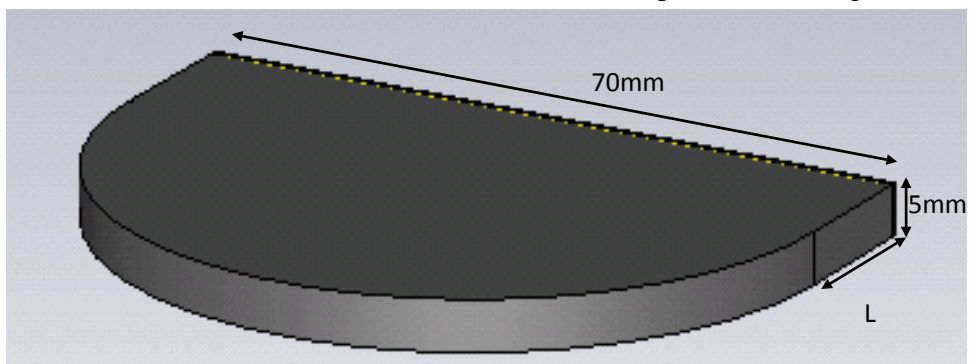


Fig. 26. Extended semi-circular lens model.

3.2.4 Simulation result of extended semi-circular lens model

Fig. 26 shows the S-parameter of the extended semi-circular lens model, covering the band from 5-30GHz. It is clear to observe that the S11 is below -10dB from 18 GHz on. In the lower frequency part, the S11 is not higher than -5dB. The impedance is shown in Fig. 28. The real part is closer to 50Ω and the imaginary part is closer to 0Ω at high frequency band compared to the ones at low frequency band. Fig. 29 shows the E-field distribution in H-plane at 30 GHz. A main beam is formed on top of the lens. In summary, the extended semi-circular lens is designed successfully according to the calculation.

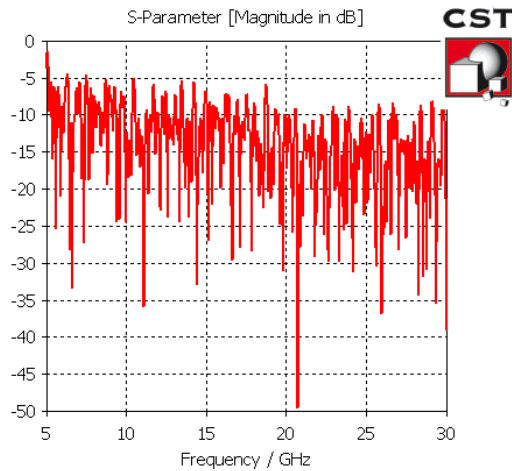


Fig. 27. S11 of extended semi-circular lens model.

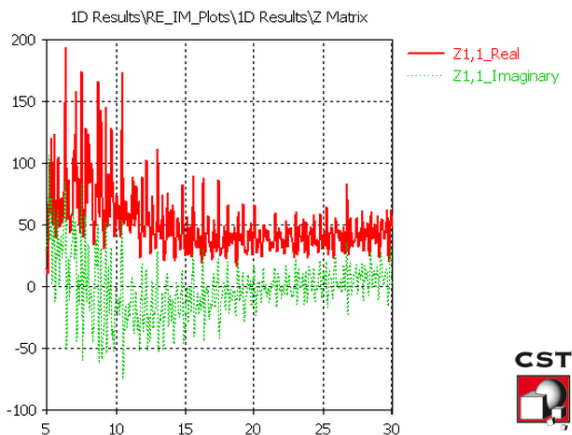


Fig. 28. Impedance of extended semi-circular lens model.

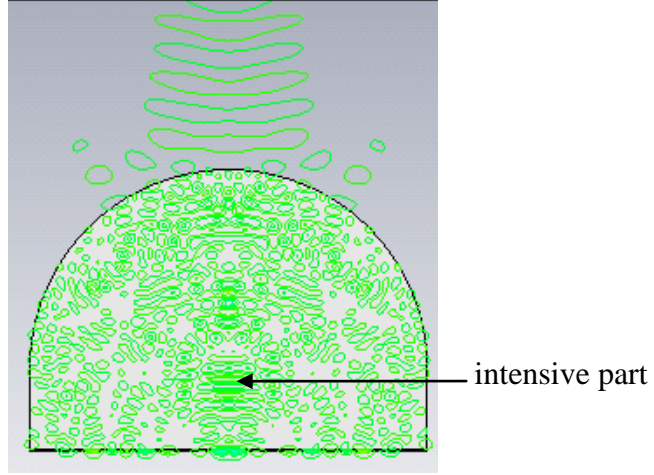


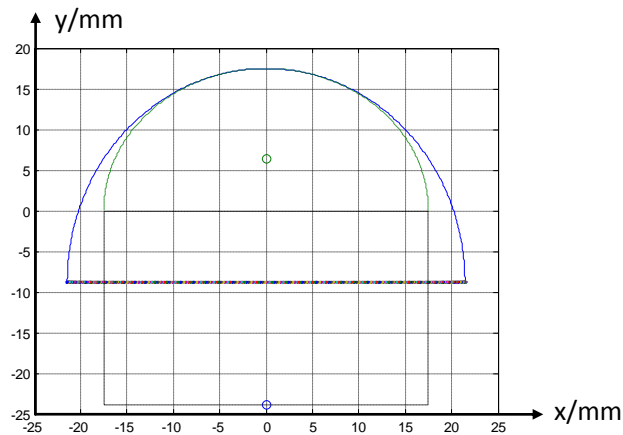
Fig. 29. Illustration of the E-field view of leaky wave propagation in the extended semi-circular lens model at 30GHz.

3.2.5 Discussion and comparison of the two types of lens

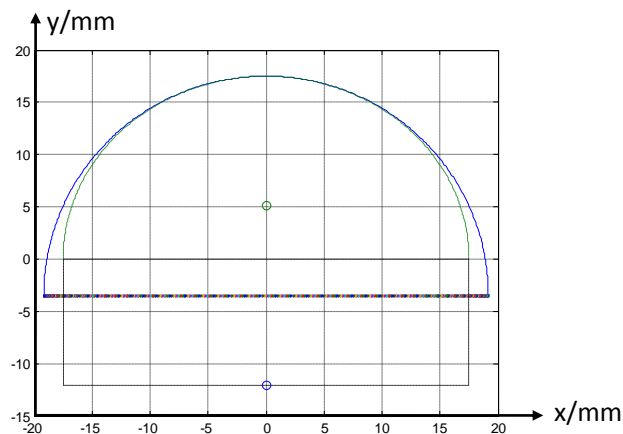
By comparing the simulation results from the two models that mentioned in chapter 3.2.2 and chapter 3.2.4, it is easy to find they are almost the same. The reason is that according to Eq. (3.20), a higher permittivity leads to a lower eccentricity. When the eccentricity is lower, the equivalent circle has a better geometrical approximation with the ellipse [25]. This conclusion can be also understood by the Fig.30. The solid line represents the ellipse and the dashed line represents the corresponding semi-circular approximation. It is clear to see that when the permittivity is increased, the two geometrical patterns are more identical. However, in the practical case, circular lens is much easier for fabrication, which is why we adopt extended semi-circular lens as the basis for matching layer design in chapter 3.3.

For most UWB communications, the linearity of the phase of the antenna transfer function is very important. The propagation constant in the dielectric k_d and the distance of observation point from the feed point r_d relate to the phase as $e^{-jk_d r_d}$ [4]. If the antenna is dispersive, compensations at system level must be included [26]. Non dispersive means the phase varies linearly with frequency. In this case, the phase center is constant and placed on top of the lens for all frequencies and observation

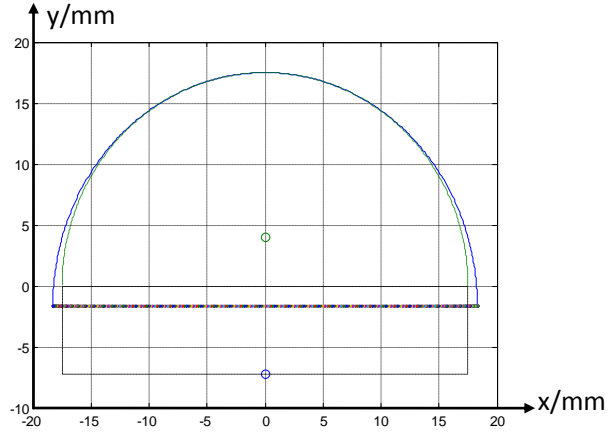
points in the main beam, and the phase variation as a function of frequency is linear, which are already proved in [4]. As a result, the leaky lens antenna could be considered as non-dispersive. Here is a contrast with the TEM-horn antenna. TEM-horn antenna has been viewed as low dispersive antenna since the phase center moves with frequency [4], and the phase linearity is only limited to the broadside direction. However, there is some drawback with the leaky lens antenna. Part of the energy is reflected back and concentrates on the focal point of the semi-circular, which explains why there is an intensive part inside lens in Fig. 29. In this way, part of energy is wasted.



$$\epsilon_{\text{lens}} = 3$$



$$\epsilon_{\text{lens}} = 6$$



$$\epsilon_{\text{lens}} = 11.67$$

Fig. 30. Comparison of approximations among different permittivities.

5.3 Matching Layer

In this chapter, the effect of matching layers is illustrated by 3 simple models, and the matching layers for leaky lens antenna is designed and simulated.

5.3.1 Theory of matching layer

In the recent years, matching layer plays an important role in the dielectric antenna design. In some references, matching layer is also referred as coat layer. The main effect of matching layer is anti-reflection [27]. In the ideal case, zero reflection could be achieved. By the three different models, the theory of anti-reflection is illustrated and contrasted as below.

For all the models in 5.3.1, we define the following parameter.

- n refractive index of the corresponding layer.
- n_a refractive index of the lens, which is assumed to $\sqrt{11.67}$
- n_b refractive index of the air, which is assumed to 1.
- η characteristic impedance of corresponding layer
- ρ elementary reflection coefficient at the corresponding interface
- l thickness of the corresponding layer

Assume the incident wave is always propagating from left side to right side.

Model A

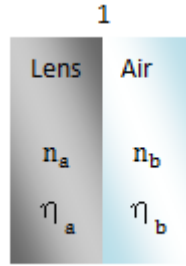


Fig. 31. Simple model without matching layer.

Fig. 31 shows a simple model without matching layer. Incident wave is propagation from lens to air. According to the equation of reflection coefficient, the reflection coefficient at interface 1 in this case should be [11]

$$\Gamma_1 = \rho = \frac{\eta_b - \eta_a}{\eta_b + \eta_a} \quad (3.26)$$

As characteristic impedance is inverse proportional to the refractive index,

$$\rho = \frac{n_a - n_b}{n_a + n_b} \approx 55\% \quad (3.27)$$

$$\rho_{\text{power}} = |\rho|^2 \approx 30\% \quad (3.28)$$

It is stated by Eq. (3.28) that without any matching layer, 30% of the energy is reflected at interface 1.

Model B

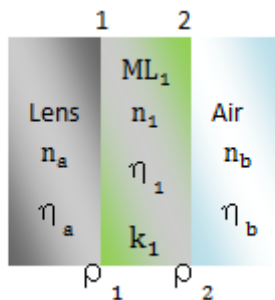


Fig. 32. Simple model with one matching layer.

Fig. 32 shows the model with one matching layer between lens and air. As it is known to us, the electric field can be decoupled into forward propagating electric field E_+ and backward propagating electric field E_- . Γ is defined as the reflection coefficient at the corresponding interface. The parameter without “'” represents the left boundary value at certain interface and the parameter with “'” represents the right boundary value at that interface. According to the matching condition for the reflection coefficient, the reflection coefficient at interface 1 should be [11],

$$\Gamma_1 = \frac{\rho_1 + \Gamma'_1}{1 + \rho_1 \Gamma'_1} \quad (3.29)$$

Due to that the tangential components of the electric and magnetic fields are continuous across the two sides of interface, which means $E = E'$. Thus

$$\Gamma'_1 = \frac{E'_{1-}}{E'_{1+}} = \frac{E_{1-}}{E_{1+}} = \Gamma_1 \quad (3.30)$$

By the equation of reflection coefficient propagation [11]

$$\Gamma_1 = \Gamma_2 e^{-2jk_1 l_1} \quad (3.31)$$

Applying Eq. (3.30) and Eq. (3.31) to Γ_1 , we obtain

$$\Gamma_1 = \frac{\rho_1 + \Gamma_2 e^{-2jk_1 l_1}}{1 + \rho_1 \Gamma_2 e^{-2jk_1 l_1}} \quad (3.32)$$

The same equation could be used in the interface 2,

$$\Gamma_2 = \frac{\rho_2 + \Gamma'_2}{1 + \rho_2 \Gamma'_2} \quad (3.33)$$

$$\Gamma'_2 = \frac{E'_{2-}}{E'_{2+}} \quad (3.34)$$

Since there is no backward wave in medium η_b , which means $E'_{2-} = \Gamma'_2 = 0$. Thus,

$$\Gamma_2 = \rho_2 \quad (3.35)$$

$$\Gamma_1 = \frac{\rho_1 + \rho_2 e^{-2jk_1 l_1}}{1 + \rho_1 \rho_2 e^{-2jk_1 l_1}} \quad (3.36)$$

In order to get the lowest reflection coefficient Γ_1 , the way is to minimize Eq. (3.36). The ideal case is to make it zero, which gives,

$$\rho_1 + \rho_2 e^{-2jk_1 l_1} = 0 \quad (3.37)$$

$$e^{2jk_1 l_1} = -\frac{\rho_2}{\rho_1} \quad (3.38)$$

As it is known to us, $e^{j\theta} = \cos \theta + i \sin \theta$. For Eq. (3.38), the left side is a complex value and the right side is a real value. The only way to satisfy this equation is to make $e^{-2jk_1 l_1} = 1$ or $e^{-2jk_1 l_1} = -1$. These two possible strategies are discussed as below. [11]

Strategy 1

Under the condition of $e^{-2jk_1 l_1} = 1$, the thickness l_1 and reflection coefficient Γ_1 are determined as follow,

$$\text{If } e^{2jk_1 l_1} = 1 \Rightarrow \rho_2 = -\rho_1, \quad 2\pi = 2k_1 l_1 = 2 * \frac{2\pi}{\lambda_1} l_1 \Leftrightarrow l_1 = \frac{\lambda_1}{2} \quad (3.39)$$

$$\frac{\eta_b - \eta_1}{\eta_b + \eta_1} = \rho_2 = -\rho_1 = \frac{\eta_a - \eta_1}{\eta_a + \eta_1} \quad (3.40)$$

Applying Eq. (3.39) and Eq. (3.40) to Eq. (3.36), we obtain

$$\Gamma_1 = \frac{\frac{-\eta_a + \eta_1}{\eta_a + \eta_1} + \frac{\eta_b - \eta_1}{\eta_b + \eta_1}}{1 + \frac{-\eta_a + \eta_1}{\eta_a + \eta_1} \cdot \frac{\eta_b - \eta_1}{\eta_b + \eta_1}} = \frac{\eta_a - \eta_b}{\eta_a + \eta_b} \quad (3.41)$$

It is stated by the Eq. (3.39) and (3.41) that the zero reflection could be achieved as long as two conditions are satisfied, 1) the thickness of the matching layer is the half-wavelength of the corresponding medium, 2) the refractive index of medium a and b are same.

However, Eq. (3.41) implies that the reflection coefficient Γ_1 is the same as if the matching layer is absent. Consequently, in strategy 1 the matching layer acts as an absentee layer and doesn't make an effect on changing the reflection coefficient.

Strategy 2

Under the condition of $e^{-2jk_1l_1} = -1$, the thickness l_1 and reflection coefficient Γ_1 are determined as follow,

$$\text{If } e^{j(2k_1l_1)} = -1 \Leftrightarrow \rho_2 = \rho_1, \quad \pi = 2k_1l_1 = 2 * 2\frac{\pi}{\lambda_1}l_1 \Leftrightarrow l_1 = \frac{\lambda_1}{4} \quad (3.42)$$

$$\frac{\eta_b - \eta_1}{\eta_b + \eta_1} = \rho_2 = \rho_1 = \frac{\eta_1 - \eta_a}{\eta_1 + \eta_a} \quad (3.43)$$

Applying Eq. (3.42), Eq. (3.43), and Eq. (3.36), we obtain

$$\Gamma_1 = \frac{\frac{\eta_1 - \eta_a}{\eta_1 + \eta_a} \frac{\eta_b - \eta_1}{\eta_b + \eta_1}}{1 - \frac{\eta_1 - \eta_a}{\eta_1 + \eta_a} \frac{\eta_b - \eta_1}{\eta_b + \eta_1}} = \frac{n_a n_b - n_1^2}{n_a n_b + n_1^2} \quad (3.44)$$

It is stated by the Eq. (3.42) and Eq. (3.44) that the zero reflection could be achieved as long as two conditions are satisfied, 1) the thickness of the matching layer is the quarter-wavelength of the corresponding medium, 2) the refractive index of medium n_1 should be equal to $\sqrt{n_a n_b}$.

It is obviously that $n_a \neq n_b$ in our case, which means strategy 1 is not suitable. In another word, the reflection coefficient is not changed by adding the half-wavelength matching layer, which indicates such matching layer plays no role in the whole structure.

Consequently, by strategy 2, as long as an appropriate thickness and material is chosen, the reflection coefficient at interface 1 is able to minimize to zero. In our example, as long as $l_1 = \lambda_1/4$ and $n_1 = \sqrt{n_a n_b}$, $\Gamma_1 = 0$ could be achieved.

$$\Gamma_{\text{power}} = |\Gamma|^2 = 0 \quad (3.45)$$

Model C

Fig. 33 shows a simple model with two matching layers. The reflection coefficient at each interface 1, 2 and 3 could be calculated by the Eq. (3.29).

$$\Gamma_1 = \frac{\rho_1 + \Gamma_2 e^{-2jk_1l_1}}{1 + \rho_1 \Gamma_2 e^{-2jk_1l_1}} \quad (3.46)$$

$$\Gamma_2 = \frac{\rho_2 + \Gamma_3 e^{-2jk_2l_2}}{1 + \rho_2 \Gamma_3 e^{-2jk_2l_2}} \quad (3.47)$$

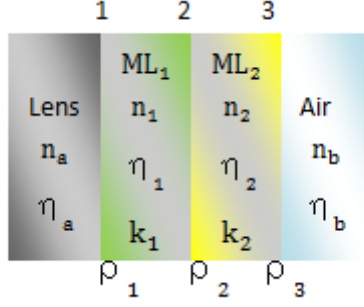


Fig. 33. Simple model with two matching layers.

As there is no backward wave in the medium η_b , thus

$$\Gamma_3 = \rho_3 \quad (3.48)$$

Applying Eq. (3.47) and Eq. (3.48) to Eq. (3.46), we obtain [11]

$$\Gamma_1 = \frac{\rho_1 + \rho_2 e^{-2jk_1 l_1} + \rho_1 \rho_2 \rho_3 e^{-2jk_2 l_2} + \rho_3 e^{-2jk_1 l_1} e^{-2jk_2 l_2}}{1 + \rho_1 \rho_2 e^{-2jk_1 l_1} + \rho_2 \rho_3 e^{-2jk_2 l_2} + \rho_1 \rho_3 e^{-2jk_1 l_1} e^{-2jk_2 l_2}} \quad (3.49)$$

Similar as the case of model B, in order to achieve zero reflection, the numerator of Eq. (3.49) should be equal to zero. However, the numerator is a complex value. Under the conditions of Eq. (3.50), which is based on the conclusion in Model B, all the imaginary parts could be removed.

$$n_1 l_1 = n_2 l_2 = \frac{\lambda_0}{4} \quad (3.50)$$

Hence Γ_1 can be written as,

$$\Gamma_1 = \frac{\rho_1 - \rho_2 - \rho_1 \rho_2 \rho_3 + \rho_3}{1 - \rho_1 \rho_2 - \rho_2 \rho_3 + \rho_1 \rho_3} \quad (3.51)$$

According to the definition of the elementary reflection coefficient,

$$\rho_1 = \frac{n_a - n_1}{n_a + n_1} \quad \rho_2 = \frac{n_1 - n_2}{n_1 + n_2} \quad \rho_3 = \frac{n_2 - n_b}{n_2 + n_b} \quad (3.52)$$

Applying Eq. (3.52) to Eq. (3.51), we obtain

$$\Gamma_1 = \frac{n_a n_2^2 - n_b n_1^2}{n_a n_2^2 + n_b n_1^2} \quad (3.53)$$

$$\Gamma_1 = 0 \Rightarrow n_a n_2^2 = n_b n_1^2 \quad (3.54)$$

Due to $n_a > n_b$, $n_2 < n_1$, which means in order to obtain zero reflection at interface 1 with two matching layers, matching layer 2 should be a less dense medium compared to matching layer 1. Based on Eq. (3.50) and (3.54) simultaneously, a system with two matching layers could be designed to meet the zero reflection requirements.

However, all the calculations above are targeted for single frequency. Because in vacuum, when frequency is changed, the wavelength will be changed at the same time, which means one thickness cannot satisfy Eq. (3.50) in whole frequency band. With the help of optimization tool box in matlab, an optimal combination of thickness and fraction index could be determined by finding the minimal average value to give the wideband system the best performance.

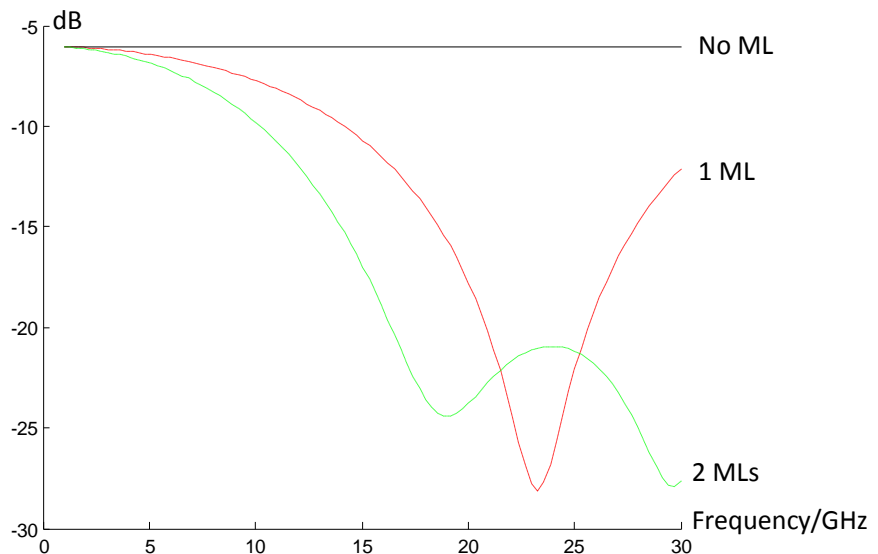


Fig. 34. Reflection coefficients comparison of different matching layers.

Fig. 34 shows the reflection coefficients at interface 1 over different numbers of matching layers. The amplitude is in dB value. The solid line represents the reflection coefficient without matching layer. The dashed curve and dash dot curve show the reflection coefficients with one matching layer (Model B) and two matching layers (Model C) respectively.

The reflection coefficient without any matching layer is around -6dB. After adding one matching layer, the overall level of the curve is lowered down significantly. The minimal value of Γ_1 of the dashed curve is approximately -27dB, at around 24GHz, which is also the perfect frequency point for one matching layer model. At this frequency, the reflection energy is only around 0.1%. However, only one matching layer doesn't help a lot in the low frequency band, especially in the frequency range 5-10 GHz. From chapter 3.1 and 3.2 we already know that the S11 performs the worst in this range, which means that the performance improvement at low frequencies is very important. It is clear to see from the dash-dot curve that by adding the second matching layer, the average level of reflection coefficient keeps going down. Especially in the low frequency band, the Γ_1 is lowered by 1 to 3 dB.

In addition, here is another defect for single matching layer. Sometimes it is hard to find a proper material according to the calculations result. In such case, if the ideal material is replaced by a similar one, the S-parameter of the whole frequency band will increase rapidly. For example in Fig. 35, when permittivity is only decreased by 0.4, the minimal value of the curve is increased by 9dB. This proves the tolerance of Model B is very weak. However, multi-matching layers can provide more combinations and possibilities, which will solve this problem efficiently.

As a result, by adding more matching layers, the reflection can be decreased efficiently in the wideband system. To widen the bandwidth, and at the same time keep the reflection response low, more than two layers must be used [11]. Fig. 36 shows the reflection coefficients with different matching layers. The dotted curve indicates the three matching layers case. Compared with the two matching layers case, the general level of the curve is successfully lowered down in the whole frequency band, especially from 5GHz to 15 GHz. Fig. 37 show the corresponding transmission coefficients. For the three matching layer model, almost all the energy are transmitted from 12GHz on, which is 4GHz lower than the two matching layer case.

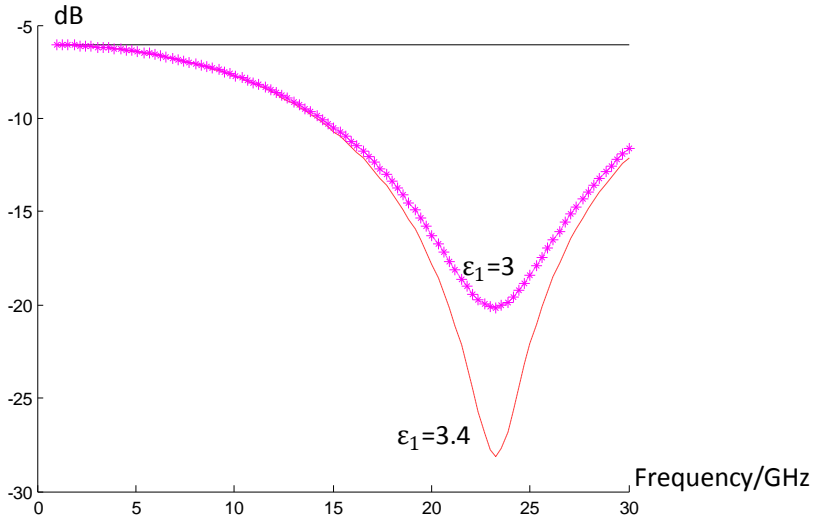


Fig. 35. Reflection coefficients of matched and de-matched single matching layer.

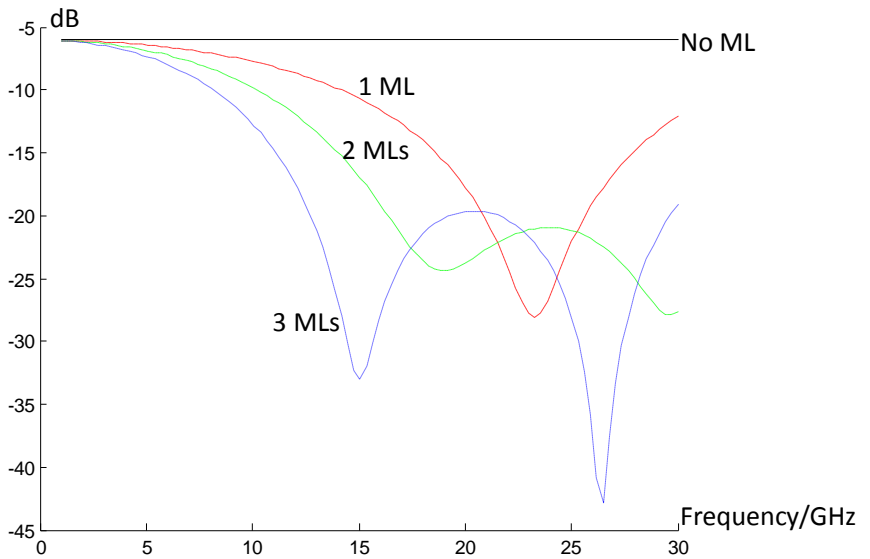


Fig. 36. Reflection coefficients with different matching layers.

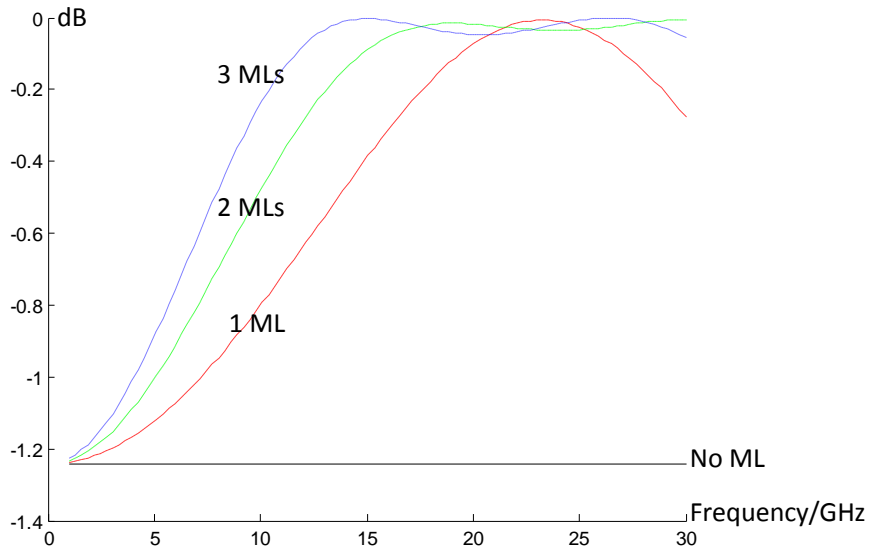


Fig. 37. Transmission coefficients with different matching layers.

Finally, an optimal combination of thickness and permittivity could be determined, which is listed in the table 2. The materials are determined according to the permittivity, which are porcelain, paper and Teflon. After adding the matching layer, the final model of leaky lens antenna with matching layers is shown in Fig. 38.

Permittivity	Thickness (mm)	Material
$\epsilon_1 = 6.8$	$t_1 = 1.18$	Porcelain
$\epsilon_2 = 3.7$	$t_2 = 1.25$	Paper
$\epsilon_3 = 2$	$t_3 = 2$	PTFE/Teflon

Table 2. Parameters of the matching layers.

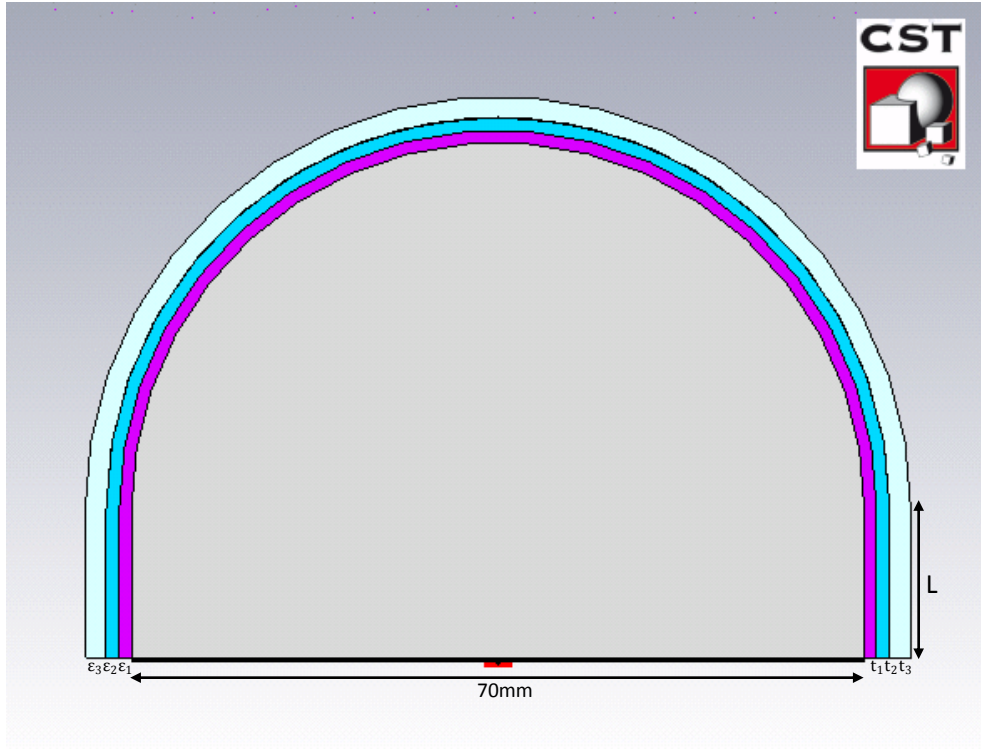


Fig. 38 Leaky lens antenna with matching layers.

3.3.2 Simulation result of the leaky lens antenna with matching layers

Fig. 39 shows the S-parameter of the leaky lens antenna with matching layers, covering the band 5-30GHz. The amplitude is in dB value. It is clear to observe that S11 is lower than -10dB from 7GHz on. Compare to the case without matching layer in chapter 3.2, the average level is decreased around 3-5 dB. Moreover, the rapid oscillation of the curve as a function of frequency is also mitigated effectively. This indicates the reflection inside the lens is alleviated. The impedance tends to be more stable during the whole frequency band, which is shown in Fig. 40. The real part is closer to 50Ω and the imaginary part is closer to 0Ω at high frequency part compared to the ones at low frequency part. The simulation results indicate that the matching layers work as expected. Additionally, Fig. 41 shows the power flow distribution comparison in the near field at 25GHz. The solid line represents the model with matching layers and the dashed line

represents the model without matching layer. It is clear to see that the power levels of the main side lobes are almost same for the two models. However, the peak value of the main lobe in the model with matching layers is more than twice as the case without matching layer. For the solid curve, the peak value of main lobe is 7529 and peak value of side lobe is 649, which means the side lobe is about 11dB lower than the main lobe. This result testifies that more power is transmitted and concentrated on the main lobe with the help of the matching layers. A power concentration on main lobe is important for UWB antenna because high directivity is required. At last, the pattern is symmetric about $x=0$.

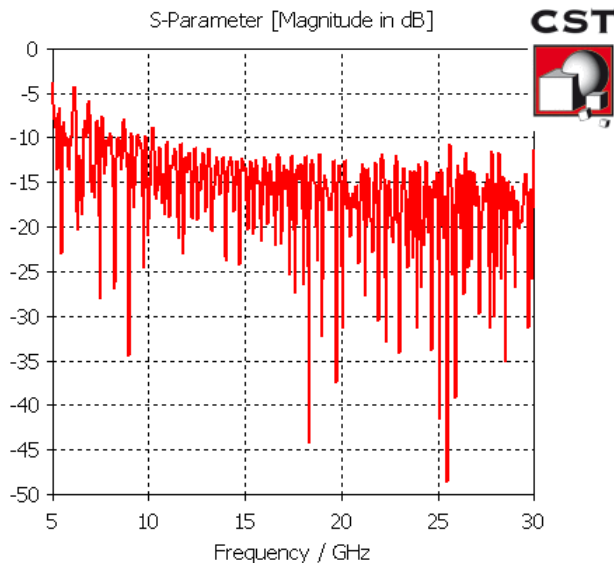


Fig. 39. S11 of leaky lens antenna with matching layers.

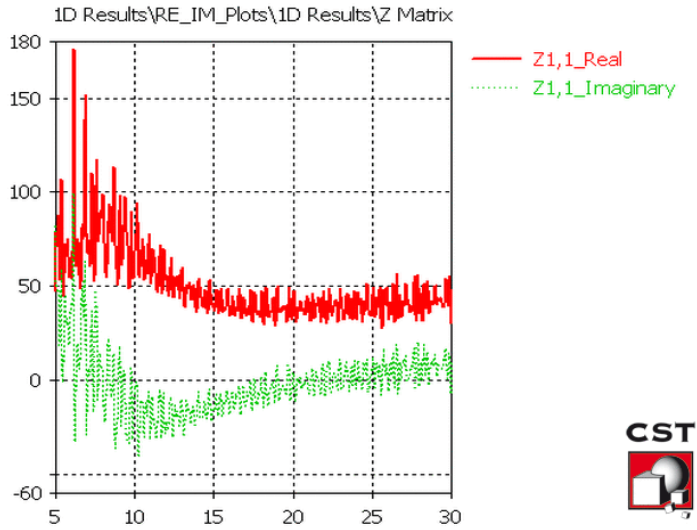


Fig. 40. Impedance of leaky lens antenna with matching layers.

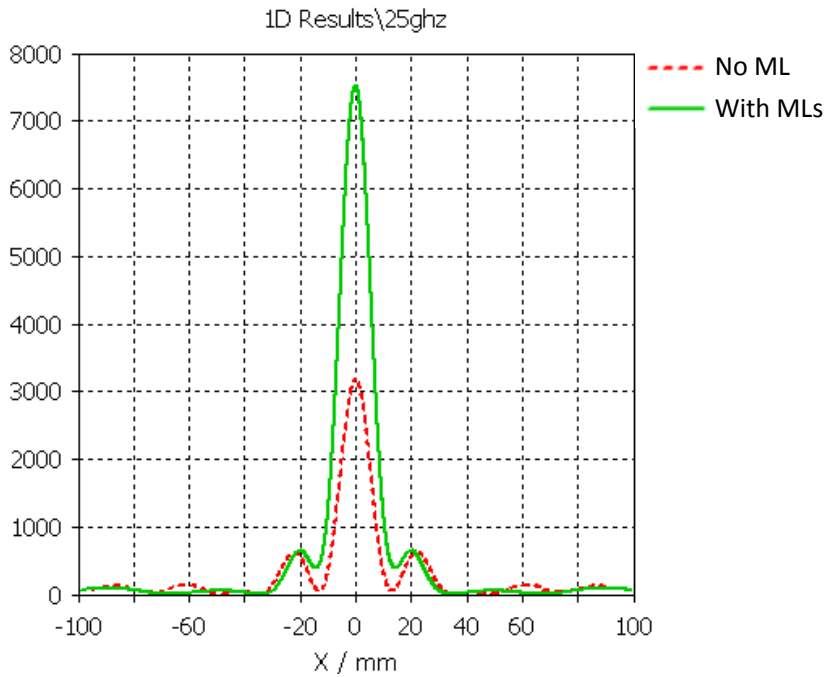


Fig. 41. Power flow distribution comparison at 25GHz.

Chapter 4

4. Conclusion and Future work

A UWB leaky lens antenna for waveguide measurements is successfully designed, modeled and simulated in the frequency range 5-30GHz. By testing the simulations result, the antenna meets the following targets:

- 1 the reflection coefficient is less than -10dB from 7GHz to 30GHz
- 2 symmetrical radiation patterns with low side lobe levels
- 3 constant phase center and low dispersion

However, the impedance matching problem deserves further discussion. In the low frequency band 5-10GHz, the antenna impedance is not matched very well. Due to the equation of impedance calculation does not take the frequency factor into account, to add some compensation structure to improve the low frequency part performance could be possible. Moreover, there may be some error between the CST simulation and real measurements. To fabricate this antenna and perform frequency and time domain measurements is essential to verify the results.

- [1] D. Cabric, M. S. W. Chen, , D. A. Sobel, J. Yang and R.W. Brodersen, "Future Wireless Systems:UWB, 60GHz, and Cognitive Radios," Custom Integrated Circuits Conference, 2005. Proceedings of the IEEE, 2005
- [2] S. Brani, A. Neto and F. Marliani, "The Ultrawideband Leaky Lens Antenna," IEEE Transactions on Antennas and Propagation, 2007
- [3] I. Vakili, "Metamaterial forward scattering measurements in a waveguide," Lund University, Master thesis, 2011
- [4] A. Neto, "UWB, Non Dispersive Radiation From the Planarly Fed Leaky Lens Antenna— Part 1: Theory and Design," IEEE Transactions on Antennas and Propagation, 2010
- [5] Y. Rahayu, T. A. Rahman, R. Ngah and P. S. Hall, "Ultra wideband technology and its applications," WOCN '08.5th IFIP International Conference on Wireless and Optical Communications Networks, 2008.
- [6] A. F. Molisch, "Wireless Communications, second edition," Wiley, 2010
- [7] H. G. Schantz, "Dispersion and UWB antennas" International Workshop on Ultra Wideband Systems, May 2004
- [8] J. D. Kraus and R. J. Marhefka, "Antennas for all applications, third edition," McGraw-Hill Science, 2002
- [9] C. A. Balanis, "Antenna Theory, Analysis and Design, second edition," John Wiley & Sons, Inc., 1997
- [10] "What is "Wavenumber?" [Online] Available:
<http://www.wavenumber.net/index.php/about>
- [11] S. J. Orfanidis, "Electromagnetic Waves and Antennas," 2008
[Online] Available: <http://www.ece.rutgers.edu/~orfanidi/ewa/>

- [12] C. F. Xie and K.J. Yao, "Electromagnetic field and electromagnetic wave," Higher Education Press, 2005
- [13] "TEM / TE / TM Fields,"[Online] Available:
<http://www.ece.utah.edu/~cfurse/microwave/LECTURE/L35%20--%20TEM,TE,TM%20waves/L35.html>
- [14] X. Y. Li, "Electromagnetic field and microwave technology," South China University of Technology Press, 1991
- [15] A. A. Oliner and D. R. Jackson, "Antenna Engineering Handbook, third edition," McGraw-Hill, 1993
- [16] D. R. Jackson and A. A. Oliner, "Modern Antenna Handbook," Wiley-Interscience, 2008
- [17] P. A. Rizzi, "Microwave Engineering," Prentice-Hall, 1987.
- [18] L. G. Maloratsky, "Reviewing the Basics of Microstrip Lines," Microw. RF, pp.79 -88, 2000
- [19] H. A. Wheeler, "Transmission-Line Properties of Parallel Strips Separated by a Dielectric Sheet," IEEE Transactions on Microwave Theory and Techniques, vol. 13, no. 2, pp. 172-185, 1965.
- [20] M. V. Schneider, "Microstrip Lines for Microwave Integrated Circuits," The Bell System Technical Journal, vol. 48, pp. 1421-1444, 1969.
- [21] E. Hammerstad and Ø. Jensen, "Accurate Models for Microstrip Computer-Aided Design," Symposium on Microwave Theory and Techniques, pp. 407-409, 1980
- [22] J. D. Kraus, "Antennas, second edition," McGraw-Hill, 1988

[23] P. Pramanick and P. Bhartia, “A generalized theory of tapered transmission line matching transformers and asymmetric couplers supporting non-TEM modes,” IEEE Transactions on Microwave Theory and Techniques, 1989

[24] “Tapered Lines,” [Online] Available:
<http://www.ittc.ku.edu/~jstiles/723/handouts/Tapered%20Lines.pdf>

[25] D.F. Filipovic “Analysis and design of dielectric-lens antennas and planar multiplier circuits for millimeter-wave applications,” University of Michigan, 1995

[26] A. Neto, S. Monni and F. Nennie, “UWB, Non Dispersive Radiation From the Planarly Fed Leaky Lens Antenna— Part 2: Theory and Design,” IEEE Transactions on Antennas and Propagation, 2010

[27] N. T. Nguyen , R. Sauleau, and C. J. M. Perez, “Very Broadband Extended Hemispherical Lenses: Role of Matching Layers for Bandwidth Enlargement,” IEEE Transactions on Antennas and Propagation, 2009